SURFACE AND INTERFACE ANALYSIS
Surf. Interface Anal. 2004; **36**: 304–310
Published online in Wiley InterScience (www.interscience.wiley.com). DOI: 10.1002/sia.1658

SIA

ToF-SIMS studies of nanoporous PMSSQ materials: kinetics and reactions in the processing of low-*K* dielectrics for ULSI applications

P. Lazzeri,[1]* G. W. Rubloff,[2] L. Vanzetti,[1] R. M. Briber,[2] M. Anderle,[1] M. Bersani,[1] J. J. Park,[2] H.-C. Kim,[3] W. Volksen,[3] R. D. Miller[3] and Z. Lin[2]

[1] ITC-irst, via Sommarive 18, 38050 Povo, Trento, Italy
[2] University of Maryland, 2145 A.V. Williams Building, College Park, MD 20742-3285, USA
[3] IBM Almaden Research Center, 650 Harry Road, San Jose, CA 95120-6099, USA

Received 1 September 2003; Revised 12 November 2003; Accepted 12 November 2003

Detailed investigations of spin-on polymethylsilsesquioxane (PMSSQ)-based low-*K* materials were carried out by means of time-of-flight secondary ion mass spectrometry (ToF-SIMS) to identify the reaction kinetics and mechanisms occurring during the manufacturing of nanoporous dielectrics for ULSI applications. Analysis of the static SIMS fingerprints led to the identification of key species related to the PMSSQ oligomers, as well to the observation of features related to the initial functionality of the precursor materials. The intensity variations of the key species with thermal curing reveal the polymerization kinetics of the dielectric precursors. In addition, thermal decomposition and volatilization of the polymethylmethacrylate–dimethylaminoethylmethacrylate copolymer (PMMA-co-DMAEMA) porogen was established based on the detection of fragments related to the different moieties of the copolymer molecule. Porogen degradation takes place via cleavage of the DMAEMA co-monomer at low temperature, followed by volatilization of the residual PMMA-enriched polymer upon annealing at higher temperature. Several complementary phenomena occurring during the formation of these complex systems can be evaluated by ToF-SIMS, revealing major features crucial to materials development and the manufacturing of novel low-dielectric-constant (*K*) dielectrics.

KEYWORDS: ToF-SIMS; PMSSQ; PMMA-co-DMAEMA; low-*K*; porogen; polymerization; kinetics; degradation

INTRODUCTION

As the feature size of ULSI devices is continuously scaled down and the packing density is augmented to boost the speed and performance of integrated circuits, the resistance–capacitance delay in interconnects becomes the factor limiting the speed of advanced circuits.

The reduction of resistance–capacitance delay to meet future needs in integrated circuit manufacturing is thus essential. With copper metallization already replacing aluminium for metal interconnects, low-dielectric-constant (low-*K*) materials are the subject of intense investigation and development to replace conventional SiO_2 dielectrics for the manufacturing of future-generation devices. The successful integration of copper and low-*K* dielectrics is the key to shortening signal propagation times in interconnects.[1]

Spin-on dielectrics have major advantages as candidates for ULSI low-*K* dielectrics. A large variety of organic or organosilicate precursors having a dielectric constant in the range $2 < K < 3$ are in fact readily available.[2] Furthermore, an additional decrease of the effective dielectric constant of these materials can be achieved by the introduction of porosity. In spin-on low-*K* materials, porosity can be obtained rather easily by adding a sacrificial porogen to the dielectric precursor.[3,4] After spin-casting, the material is annealed to promote polymerization and cross-linking of the dielectric resin. Phase aggregation followed by degradation and volatilization of the porogen takes place during curing, resulting in a network of nanopores embedded into a rigid low-*K* dielectric matrix.[5–7]

The final electrical and mechanical characteristics of the nanoporous low-*K* material depend not only on the intrinsic properties of the dielectric resin but also substantially on the size, size distribution, density and microstructure of the nanopores. However, the character of film porosity is affected by the various transformations that proceed simultaneously during processing of the material. Observation and evaluation of the transformations occurring in these systems upon curing are therefore crucial for materials development and tailoring of the fabrication process.

With these motivations in mind, we used time-of-flight secondary ion mass spectrometry (ToF-SIMS) to

*Correspondence to: P. Lazzeri, ITC-irst, via Sommarive 18, 38050 Povo, Trento, Italy. E-mail: plazzeri@itc.it

study the chemical reactions and kinetics leading to the formation of nanoporous low-*K* dielectrics. A low-*K* system of current industrial interest, based on polymethylsilsesquioxane (PMSSQ) and containing polymethylmethacrylate–dimethylaminoethylmethacrylate copolymer (PMMA-co-DMAEMA) as porogen,[8] was investigated.

EXPERIMENTAL

The PMSSQ material has the overall composition $(SiO_{1.5}CH_3)_x$ and yields amorphous dielectrics with $K < 3$. Although chemical details of PMSSQ precursors are generally proprietary, we decided to investigate two precursors from different suppliers that were supposed to be distinguishable by their initial functionality: one of the two precursors (hereafter termed 'low-SiOH') contained a lower amount of silanol groups than the other (denoted 'high-SiOH').

Solutions containing 8 wt.% PMSSQ were prepared from both precursors and mixed with the same amount of PMMA-co-DMAEMA porogen (30 wt.%). The PMMA-co-DMAEMA is a random copolymer with a monomer ratio of 75 : 25. To distinguish the chemical species clearly, fully deuterated PMMA copolymerized with conventional DMAEMA was mixed with the low-SiOH precursor.

Dielectric films ~0.5 μm thick were deposited by spin-coating, starting from these solutions, on two sets of 1″ wafers. After deposition, the samples underwent thermal annealing at 50 °C in an argon atmosphere to remove the solvent. The samples then were cured isothermally in a nitrogen atmosphere at progressively higher temperature, as reported in Table 1.

Positive and negative high-mass-resolution static SIMS spectra were acquired from these samples by a ToF-SIMS instrument (ION-TOF, ToF-SIMS IV) using a bunched 11 keV Ga^+ primary beam and probing an area 200 × 200 μm^2 in size. Negative secondary ion spectra were also collected in pseudo-dynamic SIMS conditions (termed 'pseudo-DSIMS' hereafter) after sputtering the samples with a 10 keV Cs^+ beam for a fixed time (rastered area 300 × 300 μm^2). During sputtering, one-fifth of the film thickness was removed. For pseudo-DSIMS data acquisition, a bunched 25 keV Ga^+ beam was employed. The probed area was 100 × 100 μm^2 in size. The mass resolution under these experimental conditions was 5000 at $^{28}Si^+$ and 4000 at $^{16}O^-$.

Table 1. Sample identification (D-p: porogen with deuterated PMMA; C-p: conventional porogen)

Sample	Curing temperature (°C)	Curing time (min)	Porogen
1-low-SiOH/1-high-SiOH	50	3/2	None
2-low-SiOH/2-high-SiOH	50	3/2	D-p/C-p
3-low-SiOH/3-high-SiOH	125	60	D-p/C-p
4-low-SiOH/4-high-SiOH	175	60	D-p/C-p
5-low-SiOH/5-high-SiOH	225	60	D-p/C-p
6-low-SiOH/6-high-SiOH	275	60	D-p/C-p
7-low-SiOH/7-high-SiOH	325	60	D-p/C-p
8-low-SiOH/8-high-SiOH	450	120	D-p/C-p

RESULTS AND DISCUSSION

Fingerprint analysis of PMSSQ

In Fig. 1 the negative static SIMS spectra (partial view) from the as-deposited samples 1-low-SiOH and 1-high-SiOH are displayed. The negative static SIMS spectrum from 1-low-SiOH is characterized by a sequence of regularly spaced peaks (sequence A, indicated by arrows in Fig. 1(a)) that are present in an extended mass range starting from ~250 amu up to 611 amu. At lower masses, peaks related to the matrix elemental peaks (H, C, O, Si) as well as small molecular fragments (for instance SiO_2, SiO_2CH_3) are present. Indeed, sequence A can be observed in the spectrum from sample 1-high-SiOH as well. However, the spectrum of this sample is distinguished by a second sequence (sequence B, indicated by dashed arrows in Fig. 1(b)) that consists of peaks shifted by +1.98 amu with respect to sequence A.

Two peak sequences are observed also in the positive static SIMS spectra. In particular, a single sequence characterizes the spectrum from sample 1-low-SiOH (shown in Fig. 2) and the presence of an adjoining sequence distinguishes the data obtained from sample 1-high-SiOH (not shown). The mass of the positive ions shown in Fig. 2 is

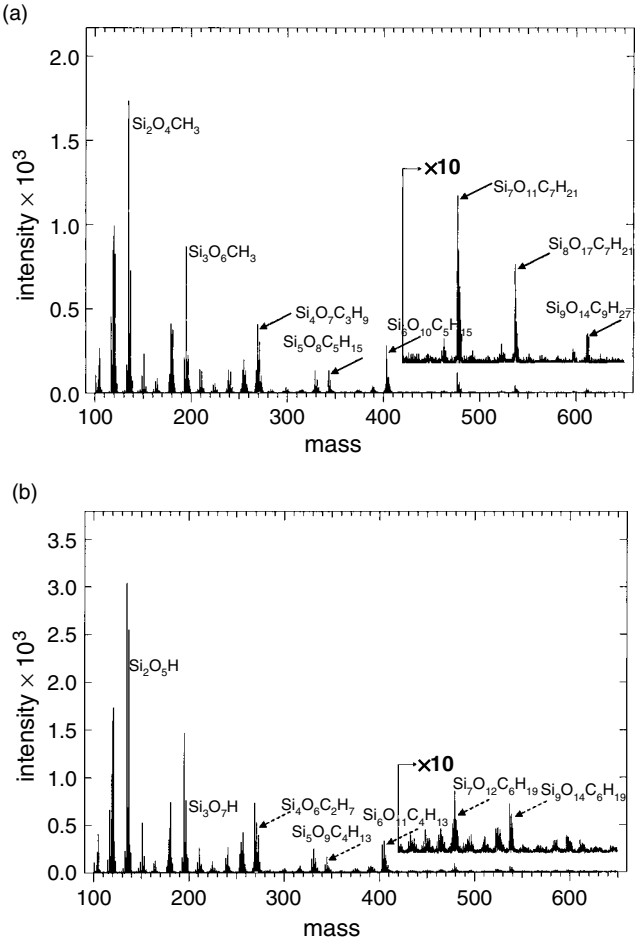

Figure 1. Negative static SIMS spectra: (a) sample 1-low-SiOH; (b) sample 1-high-SiOH.

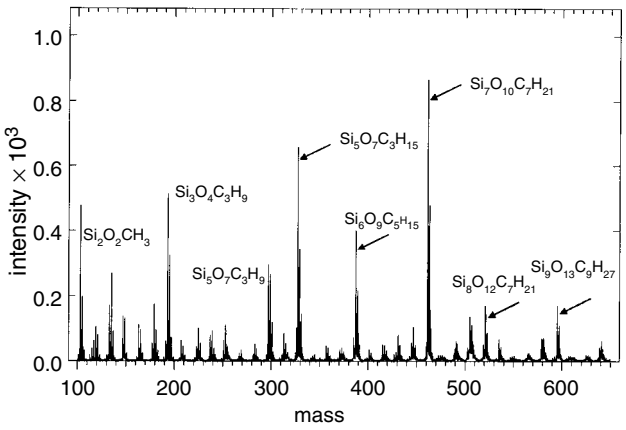

Figure 2. Positive static SIMS spectrum of sample 1-low-SiOH.

regularly shifted by −15.995 amu with regard to the mass of the peaks belonging to sequence A. Correspondingly, the positive ions distinguishing sample 1-high-SiOH are shifted by −15.995 amu with regard to the species belonging to sequence B.

The experimentally determined mass of the negative ions belonging to sequences A and B is shown in Table 2. Based on these measurements, the elemental composition and expected mass value of the corresponding species are derived. As shown by the results summarized in Table 2, good agreement is observed between the experimentally determined and the expected mass value of a series of key molecular ions containing silicon, oxygen, carbon and hydrogen. Based on these data, the molecular structure of the species belonging to sequence A is proposed (shown in Fig. 3 for exemplary fragments belonging to sequence A). The ion fragments are consistent with $SiO_{1.5}CH_3$ clusters, because in the conjectured model all the silicon atoms are bonded to a suitable number of oxygen atoms and methyl groups. In agreement with this, several peaks related to fragments arising by cleavage of these cluster ions are present in the lower region of the mass spectra.

The molecular ions shown in Fig. 3 are negatively charged so it is assumed that one oxygen atom is ionized. This assumption is fully supported by the mass of the positive ions. In fact, the mass shift of the positive ions suggests the absence of one oxygen atom (exact mass of ^{16}O is 15.9949 amu). Thus, the proposed composition of these species simply matches with a series of molecular ions having one oxygen atom less with regard to the species listed in Table 2. As a consequence, the molecular structure of the positive and negative ions is mainly the same: namely, in the positively charged ions the negatively charged oxygen atom is missing.

Similar outcomes can be obtained by measuring the exact mass of the species belonging to sequence B. However, the corresponding ions are related to molecular species having one of the methyl groups replaced by one hydroxyl group. The exact masses of CH_3 and OH are 15.0235 and 17.0027 amu, respectively. The difference between the two values (1.9792 amu) is in good agreement with the measured shift between sequences A and B. Thus, molecular ions containing unreacted OH groups clearly lead to peaks with higher intensity in the spectra from the high-SiOH material. Accordingly, a higher amount of silanol groups is expected to be present in the high-SiOH precursor.

The molecular structures displayed in Fig. 3 are adequate to explain all the peaks belonging to sequence A by the addition of a number of repeat monomeric units of formula $2(SiO_{1.5}CH_3)_n$ (where $0 \geq n \geq 2$) to base compounds containing an even or odd number of silicon atoms. The remaining peaks are often assigned to fragments related

Table 2. Conjectured identification of the negative static SIMS species

Peak sequence A			Peak sequence B		
Measured mass (amu)	Elemental composition	Expected mass (amu)	Measured mass (amu)	Elemental composition	Expected mass (amu)
268.94	$Si_4O_7C_3H_9$	268.94	270.92	$Si_4O_8C_2H_7$	270.92
342.97	$Si_5O_8C_5H_{15}$	342.96	344.96	$Si_5O_9C_4H_{13}$	344.94
402.92	$Si_6O_{10}C_5H_{15}$	402.92	404.91	$Si_6O_{11}C_4H_{13}$	404.91
476.95	$Si_7O_{11}C_7H_{21}$	476.95	478.93	$Si_7O_{12}C_6H_{19}$	478.93
536.89	$Si_8O_{13}C_7H_{21}$	536.91	538.92	$Si_8O_{14}C_6H_{19}$	538.89
610.95	$Si_9O_{14}C_9H_{27}$	610.93			

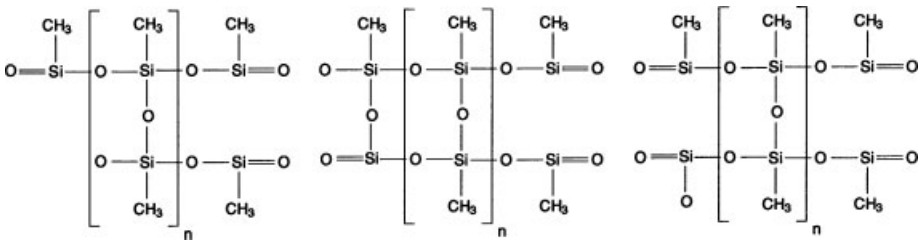

Figure 3. Molecular structures proposed for the negative ion species of sequence A.

to matrix compounds. For instance, the most intense peaks seen in the mass region below 200 amu in Fig. 1(a) are due to $Si_2O_4CH_3$ (134.96) and $Si_3O_6CH_3$ (194.96). Correspondingly, Si_2O_5H (136.93) and Si_6O_6H (196.90) are present in Fig. 1(b) and $Si_2O_2CH_3$ (102.97 amu), $Si_3O_4C_3H_9$ (192.98 amu) and $Si_5O_7C_3H_9$ (296.92 amu) can be easily recognized in Fig. 2. Other fragments are simply obtained by further cleavage of SiO_2 or CH_3 and few peaks related to minor species simply differ by the relative number of CH_3 groups and O atoms with respect to the ions belonging to sequences A and B.

All the peaks belonging to sequence B can be similarly explained, provided that the corresponding base compounds differ by the presence of the OH group. Molecular ions containing up to nine silicon atoms and a corresponding number of oxygen atoms and methyl groups are typically detected by sampling the low-SiOH as-deposited material, but species containing up to 11 silicon atoms (corresponding to $n = 3$) are clearly detected by analysing the substrate surface after low-*K* film scraping. (Film scraping was meant ideally to obtain a PMSSQ monolayer on silicon, because static SSIMS analysis of a sample monolayer is known to lead to larger molecular ions.[9]).

The relative intensity of the peaks belonging to sequence B compared with sequence A is clearly dependent on the precursor and is undoubtedly related to its initial functionality. Also, minor differences related to the features of the high-SiOH material are highlighted in the high-mass region of the spectra. In fact, the peaks characterizing the spectrum of sample 1-low-SiOH (i.e. at mass 611 amu) are hardly visible in the spectrum from 1-high-SiOH. Conversely, other ions corresponding to clusters of $SiO_{1.5}CH_3$ and containing a relatively high number of SiO_2 clusters characterize the region above mass 600 amu (not shown) of this sample. These results suggest that the high-SiOH material may be a PMSSQ–SiO_2 copolymer. As soon as the ions in the mass spectrum are related to large species, the probability that they contain assorted monomers increases. The regularly spaced fingerprint characterizing sample 1-low-SiOH is thus replaced by an irregular sequence of peaks in the high mass region of the spectrum from sample 1-high-SiOH.

The static SIMS data thus undoubtedly highlight unique features related to the PMSSQ precursors and to their characteristic functionality. With the results leading to identification of the static SIMS species and the self-consistent model supporting the proposed molecular structure, these data clearly suggest that the static SIMS key species characterizing sequences A and B are related to the PMSSQ oligomers.

Polymerization kinetics of PMSSQ

The aforementioned conclusion is clearly confirmed by the fact that the intensity of the static SIMS key peaks progressively decreases as the curing of the low-*K* material proceeds. The decrease of signal intensity observed on increasing the curing temperature is shown in Figs 4 and 5, where the negative static SIMS spectra from samples 4-low-SiOH and 8-low-SiOH are displayed.

Because it is expected that the intensity of the static SIMS peaks should not decrease upon curing if these species

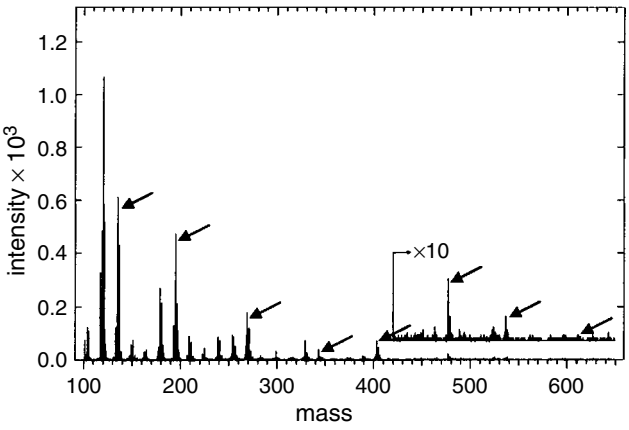

Figure 4. Negative static SIMS spectrum of sample 4-low-SiOH (175 °C, 1h).

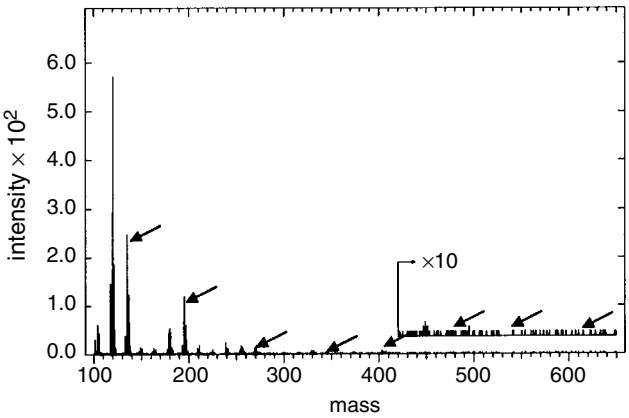

Figure 5. Negative static SIMS spectrum of sample 8-low-SiOH (450 °C, 2h).

were merely produced by the fragmentation of long MSSQ chains induced by the primary beam, it is believed that their presence provides a picture of the PMSSQ oligomer concentration. As a consequence, besides simply reflecting the characteristic features of the different precursors, it is argued that the intensity variation of these peaks can be used as a gauge of the PMSSQ polymerization kinetics. By measuring the static SIMS peak intensities, a measure of the degree of curing of the PMSSQ could thus be estimated as a function of the fabrication process conditions.[10]

The decrease in intensity of the key peaks with curing is shown by the positive static SIMS spectra as well. Moreover, if the positive and negative ions related to the same oligomer species are compared, they show a strikingly proportional intensity decrease upon curing, as displayed in Fig. 6. (As conjectured in the previous section, the negative and positive ions related to the same species simply differ in mass by one oxygen atom. In Fig. 6, the intensity of $Si_4O_7(CH_3)_3^-$, for instance, is plotted against the intensity of $Si_4O_6(CH_3)_3^+$.) Figure 6 features the data obtained by analysis of the high-SiOH samples. Closely similar results are obtained by sampling the low-SiOH samples, although some differences are observed in the relative intensity of the several species. Figure 6, remarkably, shows that all the points related to each pair of correlated species lie on a straight line, apart

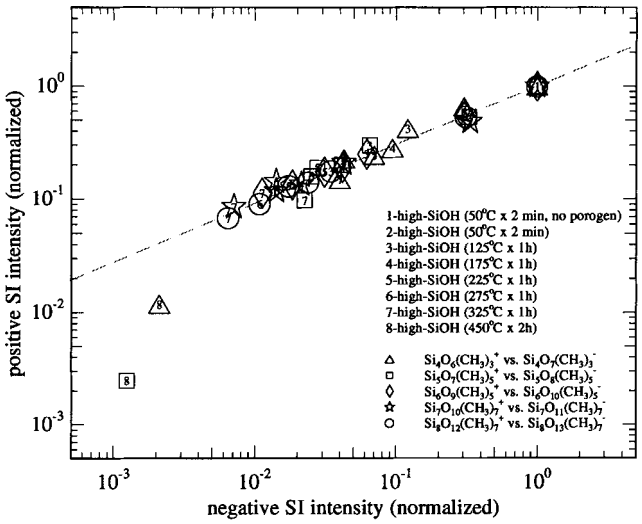

Figure 6. Intensity plot of key positive and negative species. Signals are normalized to species intensity as measured in sample 1-high-SiOH.

from some points related to sample 8-high-SiOH (due to the low intensity of the signals, being close or equal to zero in this case).

The proportional relationship between positive and negative ion signals and their progressive decrease upon curing strongly supports the hypothesis that the intensity of the static SIMS key species quantitatively reflects the PMSSQ oligomer concentration. In turn, oligomer concentration can be lowered by the presence of a certain amount of porogen and/or diminish due to progressive polymerization and cross-linking of the PMSSQ precursor upon curing. Accordingly, the intensity of the key species in 1-high-SiOH is higher than in 2-high-SiOH despite both samples undergoing annealing at 50 °C, most likely because of the presence of porogen in the latter only. Also, Fig. 6 shows that the intensity variation is higher for the negative ions. Nevertheless, either the negative or the positive static SIMS data can be used to measure the degree of curing of the PMSSQ. Indeed, preliminary results obtained by characterization of the low-SiOH and high-SiOH materials highlight different polymerization kinetics for the two precursors. Further details will be addressed in a forthcoming paper.

Porogen decomposition mechanisms and kinetics

Other peaks in the static SIMS spectra can be attributed to the porogen copolymer. In particular, by comparing the negative static SIMS spectra from the high-SiOH as-deposited and cured samples, several markers related to the porogen were recognized, including NH, CN, CH_3O, C_2O, C_4H and C_3H_3O. Based on the molecular structure of the PMMA-co-DMAEMA repeat unit displayed in Fig. 7, it can be concluded that NH and CN originate from the DMAEMA co-monomer, because only this part of the copolymer contains nitrogen. Correspondingly, CH_3O is related to PMMA because no other parts of the porogen molecule are likely to produce this fragment. The remaining peaks (C_2O, C_4H, and C_3H_3O) cannot be assigned uniquely but appear clearly related to the porogen backbone.

Some insights concerning the porogen decomposition mechanism can be derived by evaluating the intensity of these markers upon curing, even though the intensity of the negative markers is rather low. Significant signal variation was detected by comparing the marker intensity in samples cured at increasingly higher temperature, which reflects the progressive volatilization of the porogen. On the other hand, intense peaks related to the porogen, including quite large fragments (e.g. $C_4H_{10}N$), were clearly recognized in the positive static SIMS spectra. As for the negative markers, significant intensity variation with curing was observed for a number of species undoubtedly related to DMAEMA, PMMA and backbone components of the porogen. Unfortunately, rather high background values were measured for some of these markers in the spectrum from sample 1-high-SiOH. This sample does not contain porogen, meaning that unexpected organic contaminations were present that partly hid the information related to the behaviour of PMMA upon curing. As a consequence, conclusions on the porogen decomposition mechanism and kinetics were derived using some of the static SIMS data only.

The intensities of a representative number of positive and negative static SIMS markers related to the various moieties of the porogen are summarized in Fig. 8. In this plot, peak intensity is shown as a function of annealing (curing) temperature. Signals are not normalized. For comparison, the Si^+ intensity is also displayed. Based on the constant intensity of Si^+ observed over most of the curing temperature, with the only exception of sample 8-high-SiOH (annealed at 450 °C), small intensity changes are expected to bias the

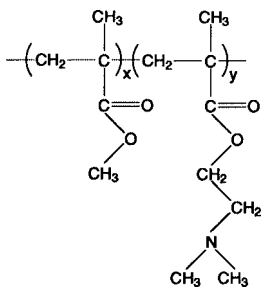

Figure 7. The PMMA-co-DMAEMA repeat unit.

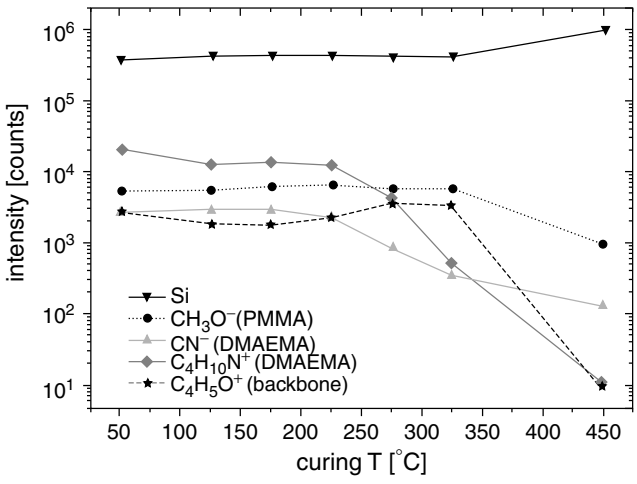

Figure 8. Intensity of porogen markers (static SIMS data).

marker peak intensity owing to the reproducibility of the experimental conditions.

As expected, owing to the lower signal intensity for the negative ions in comparison with the positive markers, the behaviour shown with curing temperature is somewhat smoother for the former. Nevertheless, the major changes in porogen marker intensity with curing are seen in both sets of data. Both markers shown in Fig. 8 related to DMAEMA (CN^- and $C_4H_{10}N^+$) exhibit a substantial decrease as soon as the annealing temperature is in excess of 225 °C. Conversely, the intensity of the markers related to the porogen backbone ($C_4H_5O^+$) and PMMA (CH_3O^-) diminishes only upon the final curing treatment at 450 °C, along with an increase of the matrix (Si^+) signal.

Moreover, very weak static SIMS signals related to the porogen were detected in the case of the low-SiOH materials. This was shown clearly to be a result of surface depletion in the porogen,[10] therefore another experimental approach to investigate porogen decomposition was attempted: namely pseudo-DSIMS spectra were acquired from the film bulk. Sputtering by Cs^+ beam was chosen to enhance the signal intensity of the organic species through matrix effects while revealing subsurface composition. Any molecular solid is damaged by sputtering exceeding the static regime so that uncertainties in interpretation of the molecular structure are generated; however, species unambiguously related to PMMA, DMAEMA and porogen backbone were recognized by comparing the data from the as-deposited and cured low-SiOH samples. Some of the prominent markers for the porogen are listed in Table 3.

Because fully deuterated PMMA was used in porogen synthesis, it can be concluded readily that deuterium and the other markers belonging to group 1 are related to PMMA. In particular, COD_3 is probably related to the PMMA co-monomer. Group 2 markers, all containing nitrogen, most likely originate from the DMAEMA co-monomer. Finally, we attribute group 3 markers to the porogen backbone as being the most likely source for large carbon clusters. In fact, carbon clusters containing hydrogen, deuterium or both are clearly detected as well, providing direct support for this hypothesis.

The intensities of some of the pseudo-DSIMS markers are shown in Fig. 9 as a function of the curing temperature. Again, the signals are not normalized. A progressive intensity increase for the matrix species is observed for the samples cured at higher temperatures, but slight signal fluctuations are observed to bias the marker intensity in this case. From Fig. 9 it is clear that the intensity for the

Table 3. Pseudo-DSIMS porogen markers

Group 1	Group 2	Group 3
D	CN	C_3
CD	C_2N	C_4
OD	C_3N	C_5
COD_3	CNO	C_6
	C_3NH	C_7
		C_8
		C_9

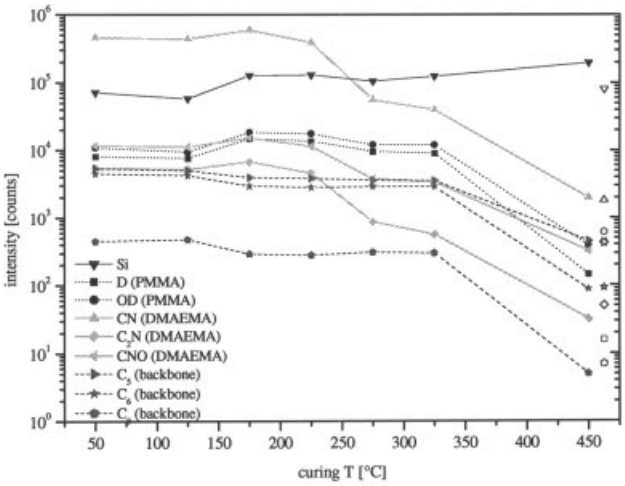

Figure 9. Intensity of porogen markers (pseudo-DSIMS data). Background values as measured in sample 1-low-SiOH are represented by hollow symbols (these data are not referred to the abscissa value).

marker related to DMAEMA (CN^-) decreases notably as soon as the annealing temperature is >225 °C. A further intensity decrease is then observed for this signal upon curing the material at higher temperatures, and finally a net intensity drop occurs upon treatment at 450 °C. In contrast, a completely different behaviour is shown by the markers related to the porogen backbone, PMMA and deuterium: the intensity of all the corresponding signals remains almost constant until the annealing temperature exceeds 325 °C, after which a clear intensity drop is observed.

By comparing the data shown in Figs 8 and 9 it can be concluded that static SIMS and pseudo-DSIMS results are in good agreement. In fact, both clearly indicate that DMAEMA co-monomer undergoes early degradation in the temperature range 225–275 °C. The by-products of this reaction must be released by the material, because the intensity of the species containing nitrogen is observed to diminish. However, the loss of DMAEMA is not complete because the intensity of the pseudo-DSIMS markers is undoubtedly higher than the background value measured in sample 1-low-SiOH (not containing porogen; intensity is shown in Fig. 9 by hollow symbols). Some DMAEMA thus appears still to be present after annealing at 325 °C, but further investigations are required to verify whether the residual signals are due to the formation of novel species.

Following DMAEMA cleavage, the porogen appears to be mainly composed of PMMA and the residual backbone structure common to both the PMMA and DMAEMA monomers. Moreover, it can be observed that the intensity of deuterium is constant until the annealing temperature exceeds 325 °C, in spite of the fact that three-eighth of ^2H is in the PMMA co-monomer. This result suggests that PMMA co-monomer is degraded only upon the final curing treatment. This conclusion is consistent with that inferred from the static SIMS markers (Fig. 8).

As a consequence of its overall thermal stability, a large amount of porogen thus remains in the materials until the annealing temperature is in excess of 325 °C, despite the fact

that cleavage of the DMAEMA co-monomer has already, at least partially, occurred. Degradation of the remaining PMMA-enriched porogen only occurs quantitatively during the final annealing treatment at 450 °C. At this point, the by-products of porogen decomposition are released as the intensity of the corresponding markers drops to the background value. These conclusions fully agree with the results obtained by thermal gravimetric/mass spectrometry studies of porogen.[8,11–12] With essentially all of the porogen lost from the film upon curing at 450 °C, the low-*K* material becomes constituted mainly by (nanoporous) MSSQ. Accordingly, the intensity of both static SIMS and pseudo-DSIMS signals associated with the matrix (i.e. Si^+) increase somewhat after the final annealing treatment.

CONCLUSIONS

The ToF-SIMS results obtained by detailed investigation of different PMSSQ precursors have highlighted several features related to complementary phenomena that occur during the fabrication of PMSSQ-based nanoporous low-*K* dielectrics.

The static SIMS spectra revealed features related to initial functionality of the precursor as well as to the behaviour of the PMSSQ oligomers upon curing. The intensity of the corresponding peaks progressively decreased as polymerization and cross-linking of the materials proceeded, providing a measure of the reaction kinetics and extent of curing of the dielectric matrix.

Furthermore, ToF-SIMS data revealed the mechanism of porogen decomposition. Both static SIMS and pseudo-DSIMS revealed details of porogen degradation pathways and their kinetics, including early initial decomposition of the DMAEMA co-monomer and the persistence of the remaining PMMA-enriched porogen until the final curing step at 450 °C. From this point of view, the pseudo-DSIMS approach was valuable in compensating for weak signals associated with surface porogen depletion (low-SiOH set) and for overcoming problems due to the presence of surface contaminant. Despite sputter damage causing a loss of information on molecular structure, the pseudo-DSIMS data provided conclusions comparable with the static SIMS results when porogen surface depletion was considerably smaller (high-SiOH set) but offered superior sensitivity over static SSIMS towards the detection of porogen - related species.

By the versatile use of ToF-SIMS, the overall reactions and kinetics leading to the formation of nanoporous low-*K* dielectrics have thus been obtained. This information is of particular value in designing nanoporous low-*K* materials and the associated processes needed for advanced interconnect technology and manufacturing. Clearly, different precursor formulations in the PMSSQ family exhibit different kinetic behaviour and interaction with the sacrificial porogen species utilized to form the nanoporous network. Furthermore, the understanding of porogen reaction pathways and kinetics also plays an important role in determining the nanostructural properties of these low-*K* dielectrics and their consequent performance in applications.

Acknowledgement

Technical support provided by N. Coghe (ITC-irst) is gratefully acknowledged.

REFERENCES

1. *The International Technology Roadmap for Semiconductors*, Semiconductor Industry Association: Santa Clara CA, 2001.
2. Peters L. *Semicond. Int.* 1998; **9**.
3. Miller RD, Hedrick JL, Yoon DY, Cook RF, Hummel JP. *MRS Bull.* 1997; **22**: 44.
4. Huang Q, Frank CW, Mecerreyes D, Miller RD. *Polym. Mater. Sci. Eng.* 2001; **84**: 792.
5. Hedrick JL, Miller RD, Hawker CJ, Carter KR, Volksen W, Yoon DY, Trollsas M. *Adv. Mater.* 1998; **10**: 1049.
6. Nguyen CV, Carter KR, Hawker CJ, Hedrick JL, Jaffe RL, Miller RD, Remenar JF, Rhee HW, Rice PM, Toney MF, Trollsas M, Yoon DY. *Chem Mater.* 1999; **11**: 3080.
7. Mikoshiba S, Hayase S. *J. Mater. Chem.* 1999; **9**: 951.
8. Huang QR, Volksen W, Huang E, Toney M, Frank CW, Miller RD. *Chem. Mater.* 2002; **14**: 3676.
9. Hagenhoff B. In *ToF-SIMS Surface Analysis by Mass Spectrometry*, Vickerman JC, Briggs D (eds). IM Publication, Chichester, UK/Surface Spectra, Manchester, UK. ISBN 1901019 039 2001; 285.
10. Lazzeri P, Vanzetti L, Iacob E, Bersani M, Anderle M, Park JJ, Lin Z, Briber RM, Rubloff GW, Miller RD. *Proc. 2003 Int. Conf. on Characterization and Metrology for ULSI Technology*, Austin, TX, 2003.
11. Huan K, Bes L, Haddleton DM, Khoshdel E, *J. Polym. Sci. A.* 2001; **39**: 1833.
12. Czégény Z, Iakab E, Blaszó, *Macromol. Mater. Eng.* 2002; **287**: 277.